University of Glasgow
DEPARTMENT OF
AEROSPACE
ENGINEERING

Numerical Simulation of Steady Supersonic and Hypersonic Flows over Simple Bodies of Revolution

D. Feszty, K.J. Badcock, B.E. Richards

Aero Report 9902

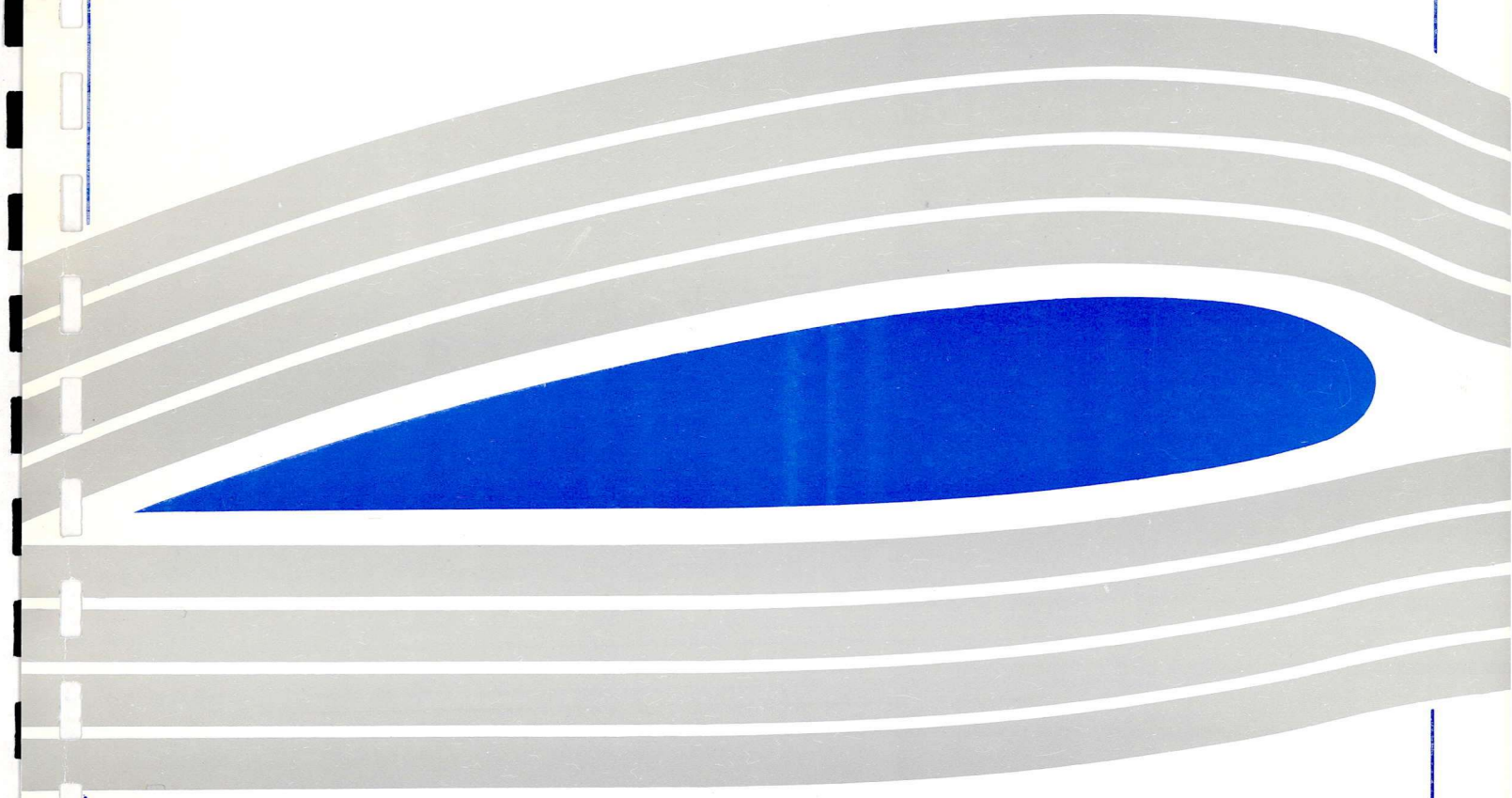

Numerical Simulation of Steady Supersonic and Hypersonic Flows over Simple Bodies of Revolution

D. Feszty, K.J. Badcock, B.E. Richards

Aero Report 9902

Numerical Simulation of Steady Supersonic and Hypersonic Flows over Simple Bodies of Revolution

D. Feszty, K.J. Badcock, B.E. Richards

Aero Report 9902,
Department of Aerospace Engineering,
University of Glasgow,
Glasgow, G12 8QQ, U.K.

March 3, 1999

Abstract

This paper reports on numerical results for supersonic and hypersonic steady flows over axisymmetric blunt bodies. Two-dimensional compressible Navier- Stokes equations are solved using a high- resolution upwind Roe's scheme. A modification to the boundary conditions and the implementation of Harten's entropy fix is proposed to improve the robustness of the code, which is then tested on an axisymmetric spike, cone and cylinder at freestream Mach numbers of 2.21, 6.00 and 30.00.

Nomenclature

D	non-dimensional blunt body diameter $\frac{D^*}{D^*}$ [1]
d	non-dimensional spike diameter $\frac{d^*}{D^*}$ [1]
M	Mach number [1]
Re	Reynolds' number, based on blunt body diameter [1]
CFL	Courant-Friedrichs-Lewy number [1]
V	non dimensional velocity $\frac{V^*}{V_{\infty^*}}$ [1]
a	non-dimensional blunt body radius $\frac{a^*}{D^*}$ [1]
c_p	pressure coefficient [1]
k	ratio of pressures in front of and behind a shock wave [1]
p	non-dimensional pressure $\frac{p^*}{\rho_{\infty^*} V_{\infty^*2}}$ [1]
Φ	blunt body half-cone angle [^{o}]
δ	non-dimensional shock detachment distance $\frac{\delta^*}{D^*}$ [1]
γ	specific heat ratio [1]
ρ	non-dimensional density $\frac{\rho^*}{\rho_{\infty^*}}$ [1]

Suffices

$*$	dimensional quantities
∞	free-stream value
$1, 2$	first and second cell values next to a wall
$G1, G2$	first and second ghost cell values outside the computational domain

1 Introduction

Computational Fluid Dynamics offers new perspectives in examining flow situations demanding high-level experimental facilities. One of the features which is of particular interest in numerical investigations is the simulation of high-speed reentry configurations involving unsteady flows [1] [2] [3].

The computational solution of such flows requires robustness from the numerical method which must have the ability to simulate the very strong bow shocks and strong expansions arising in hypersonic flow near the large angle corner of blunt bodies. The PMB2D [1] code, which has been widely used and validated for a range of supersonic freestream velocities, had encountered difficulties when solving flows with freestream Mach numbers greater than 5.

In order to identify the problems causing this, simple bodies of revolution are examined in the present investigation. The chosen bodies, a spike, a cone and a flat-nosed cylinder, ranging from a sharp-nosed to a totally blunt body, cover the whole spectrum of the flow types arising at high speeds. Their simplicity also facilitates the identification of problems, and furthermore, are representative of spiked blunt body configurations suitable for the investigation of unsteady flows.

Therefore, the present paper's aim is to report on

[1]

numerical results for supersonic/hypersonic steady flows past single blunt bodies of revolution, and through this to extend the range of problem solvable by PMB2D to very high Mach numbers.

2 Test Cases

The choice of the three simple bodies is based on tests done in [4], in which the freestream Mach numbers were 2.21 and 6.00 at a Reynolds' numbers (based on the cone/cylinder diameter) of 0.12 and 0.13 million, respectively.

The $d = 0.0065$ diameter spike with a 15^o half-angle cone forebody is a sharp nosed body and results in attached shocks and weak expansions at the shoulder at all speeds. The 50^o half-angle cone with the diameter of $D = 1.0$ results in detached shock-waves at low Mach numbers and attached at high Mach numbers, while the expansion taking place after the body shoulder is of medium strength. The flat-nosed cylinder ($D = 1.0$ again) represents the most difficult case to be solved, as it should result in a detached, very strong bow shock and strong expansion at all Mach numbers. In all cases the flow was axisymmetric at zero angle of incidence.

3 Simulation Method

3.1 Grid Generation

Two-dimensional multiblock grids for the three bodies were generated (Figs.1, 2, 3). The grid for the spike has 100x100 cells in 4 blocks, while for the cone and cylinder there are 200x50 cells chosen in 3 blocks. The gridlines are clustered towards the wall of the bodies enabling both inviscid and viscous calculations. Only every second gridline is shown in the figures.

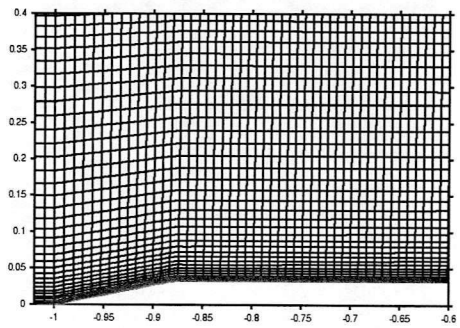

Figure 1: Grid of the spike: Detail for the spike tip

3.2 Numerical Method

The PMB2D code was used for the numerical calculations. This employs a cell-centered finite volume discretisation method to solve the Euler and Navier-Stokes

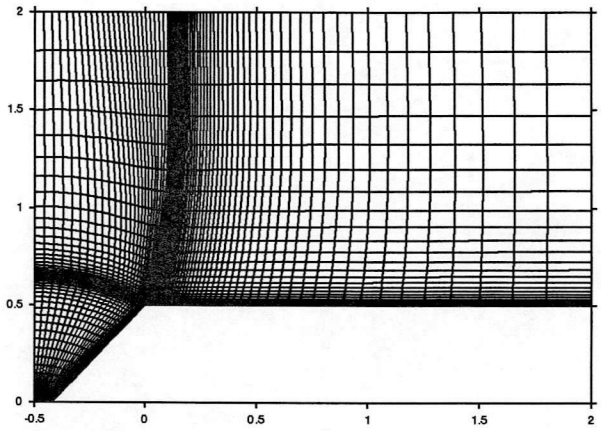

Figure 2: Grid for the 50^o cone

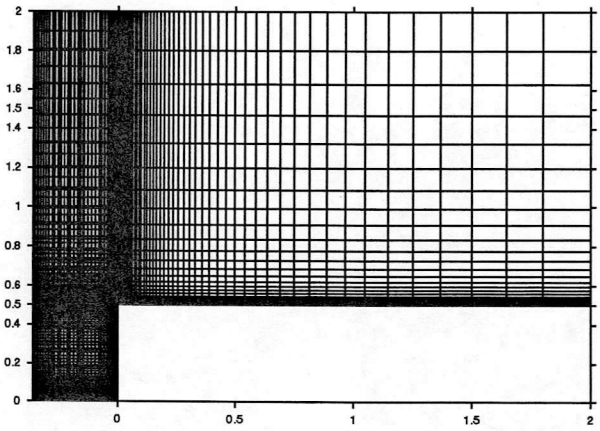

Figure 3: Grid for the cylinder

equations. A multiblock structured grid framework is applied to enable complex configuration to be tackled. An axisymmetric version of the code was used in this study. Roe's scheme with MUSCL variable interpolation is employed to discretise the convective terms and central differencing for the diffusive terms. A steady state calculation proceeds in two phases, where the freestream starting solution is smoothed out using an explicit scheme and then an implicit scheme is used to obtain rapid convergence. The linear system arising at each implicit time step is solved using a Generalised Conjugate Gradient method and a BILU factorisation is used as a preconditioner. An important feature of the code is the use of approximate Jacobian matrices for the left hand side of the linear system. The k-ω turbulent model is also implemented. The unsteady part of the code, not used in this study, employs a time-accurate pseudo time method. More details are given in [5] [6] [7].

The computations were carried out on a single 200 MHz Pentium Pro 686 processor.

3.3 Modification of the Boundary Conditions

Preliminary calculations of the supersonic flow around sharp-corner single bodies failed in the inviscid case but converged in the viscous. The failure appeared as negative pressure immediately after the body shoulder in the cells adjacent to the wall. This suggested, that the problem is associated with the boundary conditions, which differ for the inviscid and viscous cases and with the strong expansion taking place immediately after the shoulder of the sharp-corner bodies.

In the inviscid case, where a slip boundary condition is applied at the solid wall this expansion appears as a fan of expansion waves. The pressure gradient inside this fan can become very large in the direction perpendicular to the freestream velocity, the pressure gradually decreasing to almost zero in the cells adjacent to the wall. As the values of the ghost cells (which are outside the computational domain and are used by the upwind scheme - Fig.4) are calculated by a linear extrapolation of the first two cell values, they may result in significantly negative pressures because of this large gradient. When the scheme starts to calculate the new values for the computational domain, the negative ghost cell pressures involved in the computation may easily cause negative values in the first cell adjacent to the wall. The code then fails because of the negative pressure in the computational domain.

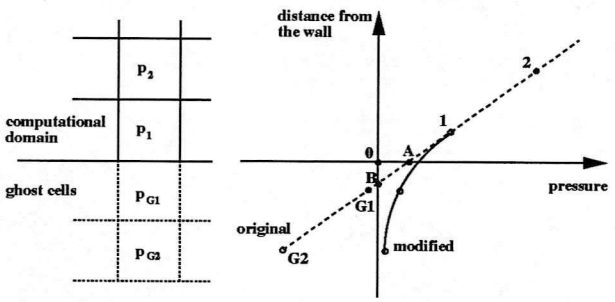

Figure 4: Modified extrapolation of the ghost cell values

On the other hand, the no-slip boundary condition at the wall employed for the viscous calculations results in low speed and therefore higher pressure values in the cells adjacent to the wall. This yields a smaller pressure gradient inside the expansion fan and thus the failure caused by a negative pressure is avoided. However, the problem encountered for inviscid flows could arise for viscous flows at very high Mach numbers.

There are two possibilities to avoid the above problem. First is the movement of points G1 and G2 into the region AB, where the pressure/density is already positive. This could be achieved by using ghost cell sizes small enough to fit into the region of height 0B. As the current method creates the ghost cells by mirroring the first two cells of the computational domain just over the boundary, the desired sizes could be obtained only by a more intense clustering of the grid near the wall. However, as the resolution of the rest of the computational domain requires still the same spacing as before, it would imply the need for more cells in the boundary region. This, in turn, would result in overall more cells than before and therefore longer calculation times.

Tests showed that using an order of magnitude smaller spacing (10 cells instead of the previously used 1) allows the calculations to run without failure, but with negative values in the second ghost cells (G2 in Fig.4) which remain there during the whole computation. Further clustering of the grid, using 40 cells instead of the originally used 1, leads to negative ghost cell values in the initial phases of the calculations only (at around 100-200 explicit steps).

The second solution is to modify the negative ghost cell values to small positive ones. This can be achieved by taking 5% of the neighbouring value instead of the value from linear extrapolation. Namely, if $p_{G1} < 0$, then $p_{G1} = 0.05p_1$ and to calculate p_{G2} we continue with the linear extrapolation. If this results in $p_{G2} < 0$ then we similarly set $p_{G2} = 0.05p_{G1}$. As the density usually changes in the same way as the pressure, we apply the same modification method.

The advantage of the second method is that there is no need to increase the number of cells in the grid thus not increasing the computational time. In the following calculations, therefore, the method of ghost cell values modification is used and its performance monitored.

3.4 The Entropy Fix

Although the modification of the boundary conditions made the code more robust, failure caused by negative pressure appeared again at the preliminary hypersonic calculations of the above bodies, this time located approximately after the strong bow shock. This seemed due to the treatment of the transient movement of this strong shock wave at the initial phases of the calculation, and therefore an entropy fix suggested in [8] was implemented in the code.

4 Verification of the Numerical Method

Grid dependence tests were carried out in order to ensure the reliability of the results. A coarse (number of gridpoints in each direction is halved) and a fine (number of gridpoints in each direction is doubled) grid were created for each case and the c_p distributions along the cylinder and the Mach contour plots were compared.

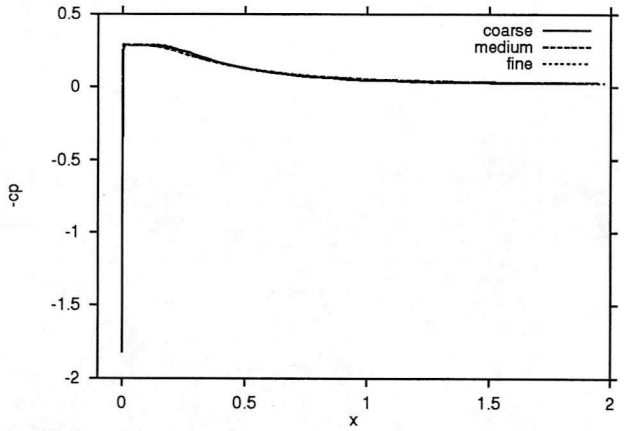

Figure 5: Grid dependence test for the inviscid flat-nosed cylinder, M=2.21

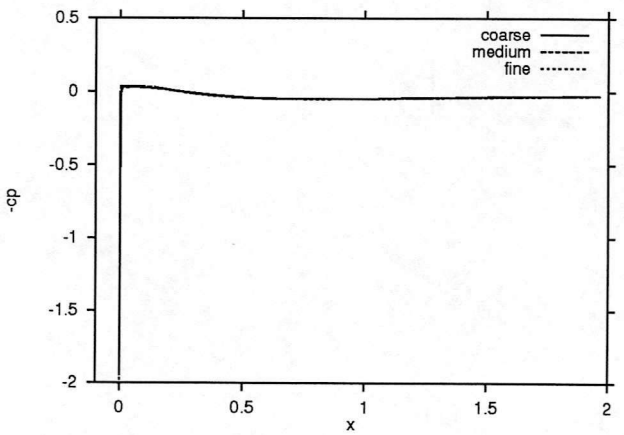

Figure 6: Grid dependence test for the inviscid flat-nosed cylinder, M=6.00

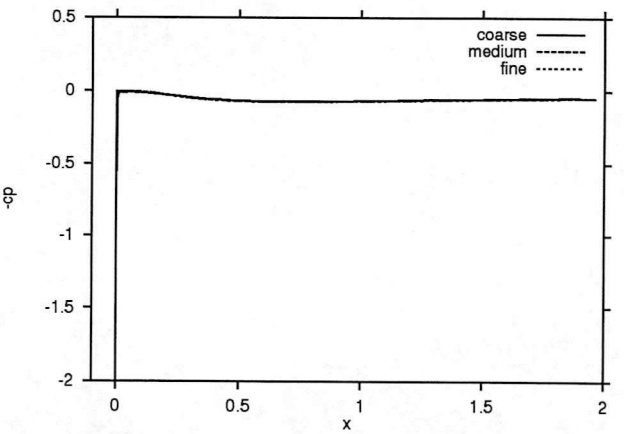

Figure 7: Grid dependence test for the inviscid flat-nosed cylinder, M=30.00

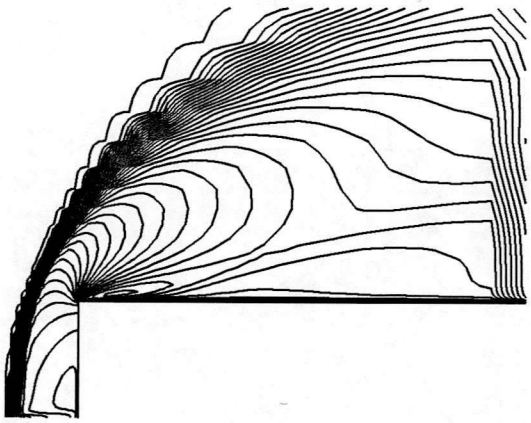

Figure 8: Mach contours obtained on coarse grid for the Mach 6.00 inviscid cylinder

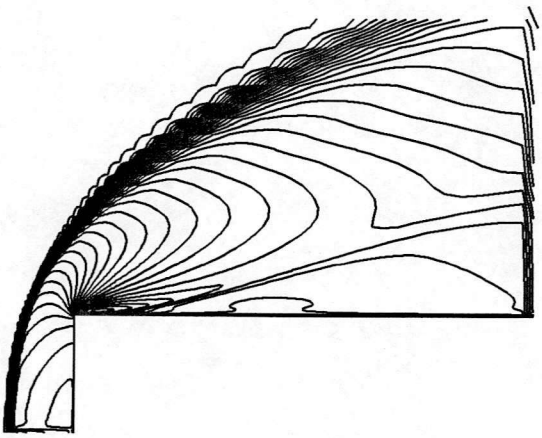

Figure 9: Mach contours obtained on medium grid for the Mach 6.00 inviscid cylinder

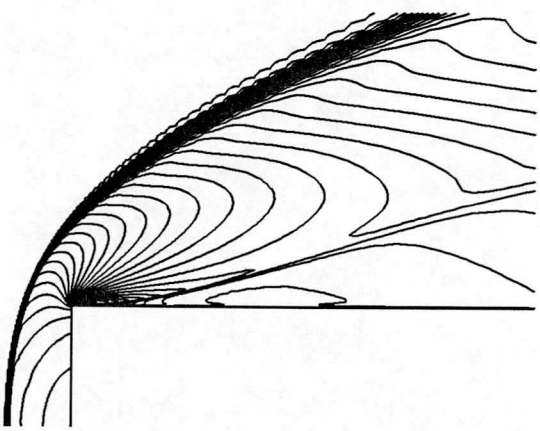

Figure 10: Mach contours obtained on fine grid for the Mach 6.00 inviscid cylinder

The inviscid cylinder at M=2.21, M=6 and M=30 were selected for these tests, as they are the most difficult from the after-corner expansion point of view and the inviscid nature makes them suitable for examining the wall boundary condition modification. The c_p distributions for all three grids at each freestream Mach number are shown in figures 5, 6, 7. To compare the Mach contours on each grid, the Mach 6.00 case was chosen (Figs. 8, 9, 10). While the c_p distributions are almost identical, the Mach contour plots manifest certain difference in the shock resolution - the finer the grid, the thinner is the shock. The waviness seen in the bow shock waves in Figs. 8-10 is concerned with the plotting routine and the coarseness of the grid and is normal in presentation of such data. However, the shape of the shock is the same in all cases.

The grid refinement has no effect on the results, and as the other geometries represent easier cases, the above conclusions on the grid refinement independence should be true for them as well. However, to avoid too thick shocks (occurring on the coarse grid) or too expensive calculations (there are 4 times more cells in the fine grid than in the medium), the medium grid was chosen for further computations.

5 Calculation Results and Validation

5.1 Spike at Mach 2.21 and Mach 6.00

Both the inviscid and laminar calculations for the spike converged rapidly in the supersonic case requiring typically 500 explicit steps at 0.4 explicit CFL and 375 implicit steps at a CFL number of 50 (marked as 500/0.4 +375/50 in the following) taking 31 minutes on the above 200 MHz Pentium Pro 686 processor. The hypersonic case converged even more rapidly with the parameters of 500/0.4+58/50 requiring only 13 minutes running time. All calculations had 3rd order accuracy and the Mach contour plots for the viscous cases are shown in Figs. 11 and 12.

Note that in the hypersonic case the shock wave angle is lower and the boundary layer is much thicker than in the supersonic. This means, that the flow is conical only at the spike tip section and hence it is interacting with the high freestream velocity causing the weak shock angle to be determined rather by the thick boundary layer than the conical spike tip.

Because of the weak strength of the expansion the boundary modification was not in use in these cases.

5.2 Cone and Cylinder at Mach2.21

All the calculations of the supersonic cases converged well with the details shown in Table 1 (3rd order accuracy again) and taking the time of 35 minutes for both 50^o cone cases and 2 h 04 minutes and 2 h 53 minutes for the inviscid and laminar cylinder, respectively.

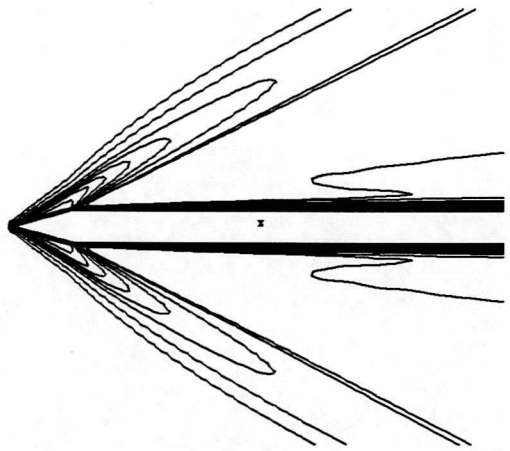

Figure 11: Mach contours for the spike, Mach 2.21, Re=0.13 million

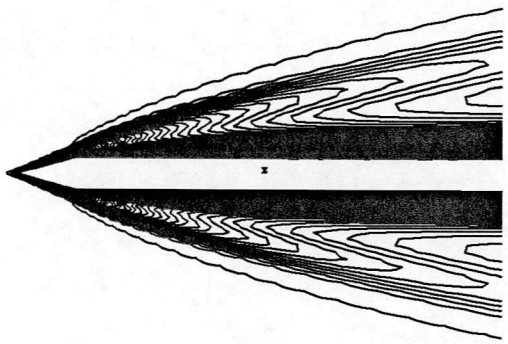

Figure 12: Mach contours for the spike, Mach 6, Re=0.13 million

Mach num.	Cone Angle	Flow Type	Explicit Steps	Implicit Steps	log Res
2.21	50	invisc.	1200/0.4	462/10	-8
2.21	90	invisc.	1500/0.4	1841/10	-8
2.21	50	lamin.	500/0.4	544/10	-8
2.21	90	lamin.	1500/0.4	2260/10	-8

Table 1: Mach 2.21 Calculation Details

Mach contour plots are shown in Figs.13,14, 16,17. As expected, the flow is detached in the cone case as the detachment angle at M=2.21 is 43.1^o [10]. The inviscid flows show an overexpanded flow right after the shoulder which recompresses in a shock-wave, while

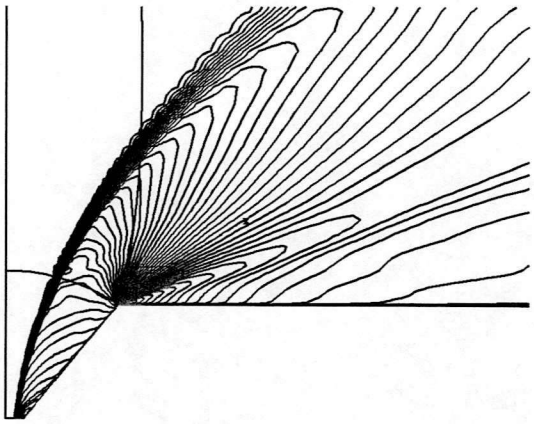

Figure 13: Mach contours for the cone, Mach 2.21, inviscid

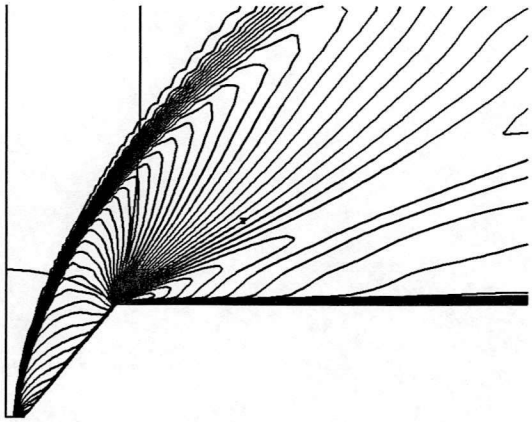

Figure 16: Mach contours for the cylinder, Mach 2.21, Re=0.13 million

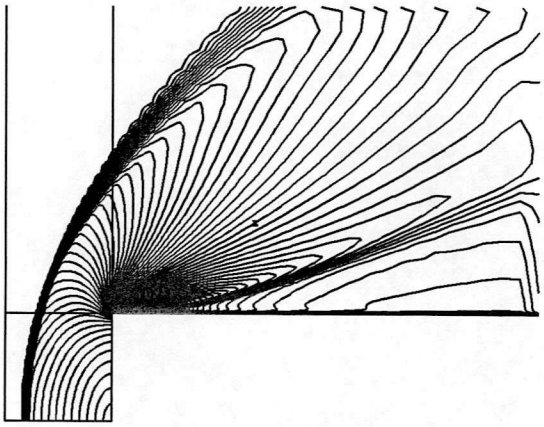

Figure 14: Mach contours for the cylinder, Mach 2.21, inviscid

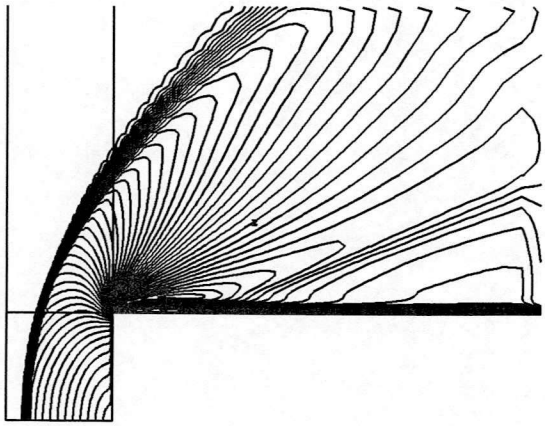

Figure 17: Mach contours for the cylinder, Mach 2.21, Re=0.13 million

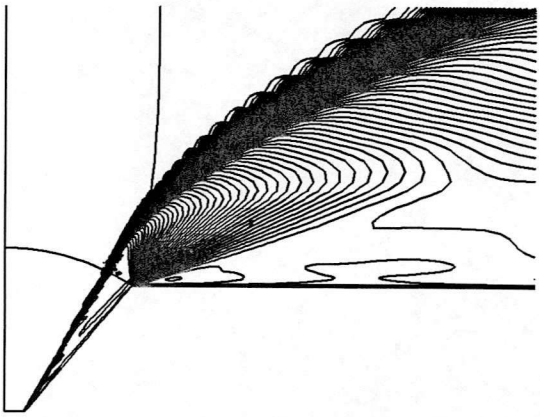

Figure 15: Mach contours for the cone, Mach 6, inviscid

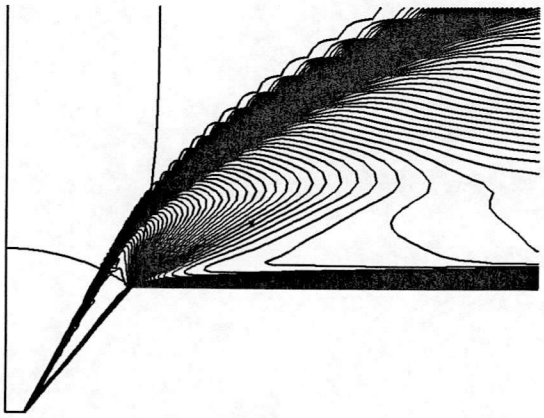

Figure 18: Mach contours for the cone, Mach 6, Re=0.13 million

the viscous flows also have overexpansion and recompression, but less evident. This is due to the influence of the boundary layer, which causes the flow to be less energetic after the corner and causes the above phenomenon to be weaker.

In addition, the behaviour of the wall boundary modification was monitored, which showed, that it was active at the initial phases of the calculations only. This means that the converged solutions would be unaffected by the modification.

5.3 Cone and Cylinder at Mach 6.00

The hypersonic flow calculations converged well in both inviscid and viscous cases (Table 2). Although the inviscid cylinder case was able to reduce the residual by -4.5 order, this is a sufficient level of convergence. These hypersonic calculations for the cylinder are generally much longer than for the supersonic case, which is caused probably by the much larger deviation in the cell values throughout the computational domain. The calculation times were 25 minutes and 1 h 45 minutes for the inviscid and laminar cone cases, and 48 and 1 h 30 minutes for the inviscid and viscous cylinder, respectively.

Mach contour plots for these cases are shown in Figs.15- 22. Note that in contrast to the supersonic case, the shock wave is attached in the cone case, as the shock-detachment angle at M=6 is 55.5°. The shock-detachment distance compared to the Mach 2.21 case is decreased for the cylinder and the boundary layers are also thicker, which agree with the theory of high-speed flows.

Mach num.	Cone Angle	Flow Type	Explicit Steps	Implicit Steps	log Res
6.00	50	invisc.	1300/0.4	180/10	-8
6.00	90	invisc.	5000/0.1	1000/3	-4.5
6.00	50	lamin.	1500/0.1	447/10	-8
6.00	90	lamin.	2000/0.4	1139/5	-8

Table 2: Mach 6.00 Calculation Details

In general, the boundary modification was active in the initial phases of the calculations only (at around 150-200 explicit steps), apart from the not fully converged inviscid cylinder case, where it remained in use during the whole computation. However, in this particular case grid clustering in the boundary region (described in section 3.3) was tested as well, but resulting in the same convergence behaviour. This shows, that the reason for this lack of convergence is somewhere else than in the proposed boundary modification.

5.4 Cone and Cylinder at Mach 30

The robustness of the proposed modifications was tested at higher hypersonic Mach numbers. The cone and the cylinder were examined at a freestream velocity of Mach 30 - a range, which was not solvable with the unmodified method. The modified code proved capable of dealing with these cases as well. However, the CFL numbers had to be chosen very carefully, which resulted in even longer calculation times than for the lower hypersonic speed Table 3. The inviscid cases required 27 minutes and 1 h 58 minutes runtime for the cone and the cylinder, respectively, whereas the laminar cases were much longer, 4 h 54 minutes and 5 h 27 minutes.

Note, that the inviscid cylinder case was again not fully converged. It seems, that certain cell value fluctuations take place in high-speed calculations and are strengthened by further increase of the speed. As the wall boundary condition modification was still active even at the late phases of this calculation, the above fluctuations could be caused by itself. However, as this problem doesn't appear at the 50° cone case, it is deduced that it is also associated with the angle of the sharp-corner shoulder and therefore with the strength of the expansion, which is also weakened by the existence of the viscosity.

M	Cone Angle	Flow Type	Explicit Steps	Implicit Steps	log Res
30	50	invisc.	1500/0.4	148/10	-8
30	90	invisc.	4000/0.1	1500/5	-2.5
30	50	lamin.	1500/0.05	5000/10 +588/200	-8
30	90	lamin.	5000/0.05	2000/2 +2800/50	-8

Table 3: Mach 30 Calculation Details

Mach contour plots in Figs.20-24 show, that the shock-wave of the 50°cone is attached once again (shock-detachment angle for M=30 is 57.5° but in the inviscid case only. On the other hand, viscous case shows a slightly detached curved shock, which is due to the relatively high Reynolds' number at this speed, causing a very thick boundary layer resulting in displacement effect. This thick boundary layer growing after the body shoulder also makes the recompression shock-wave (which is clearly visible in the inviscid cases, Fig.21) almost disappear. The shock detachment distance in the cylinder cases remains basically the same as it was for the supersonic freestream, being in agreement with the theoretical hypersonic independence for blunt shapes.

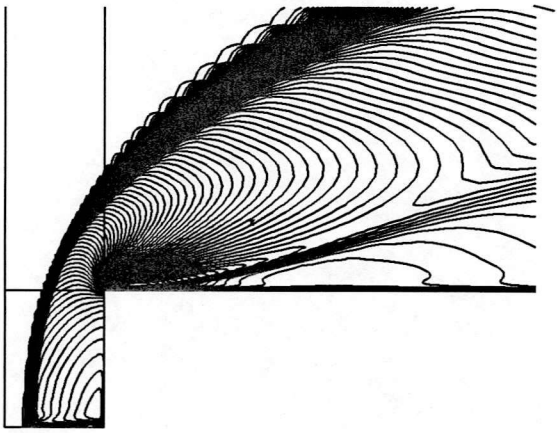

Figure 19: Mach contours for the cylinder, Mach 6, inviscid

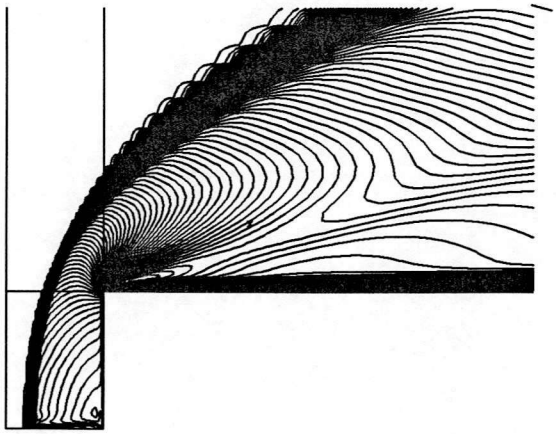

Figure 22: Mach contours for the cylinder, Mach 6, Re=0.13 million

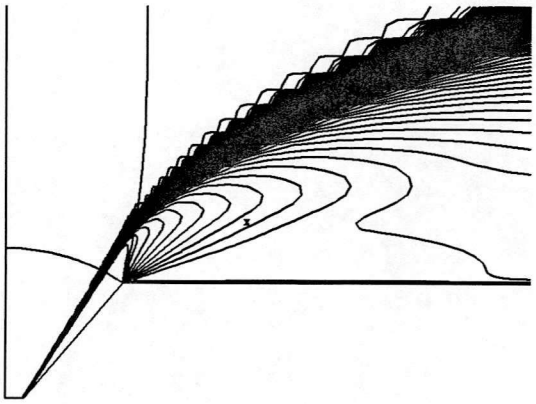

Figure 20: Mach contours for the cone, Mach 30, inviscid

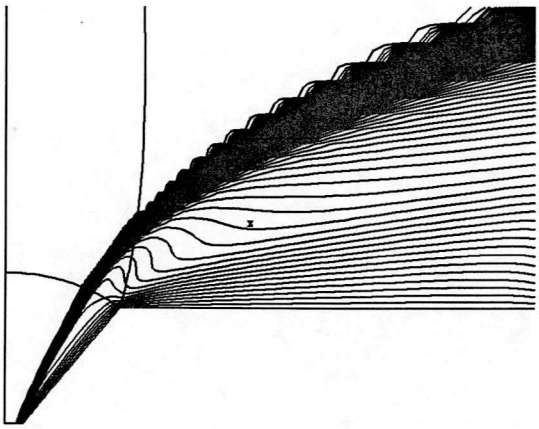

Figure 23: Mach contours for the cone, Mach 30, Re=0.13 million

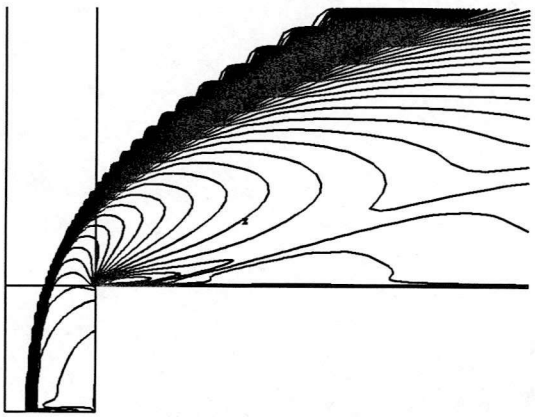

Figure 21: Mach contours for the cylinder, Mach 30, inviscid

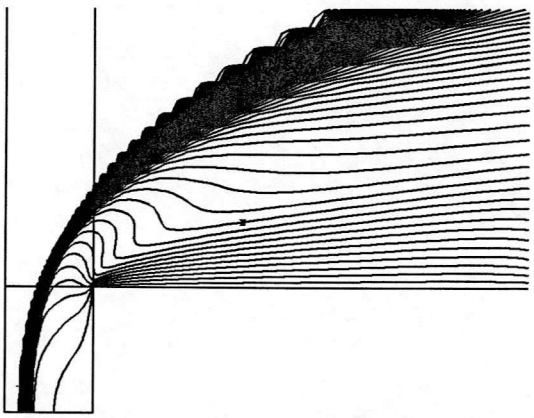

Figure 24: Mach contours for the cylinder, Mach 30, Re=0.13 million

Generally, the wall boundary condition modification was in use in the initial phases of the calculations only, apart from the not fully converged inviscid cylinder case mentioned earlier.

5.5 Results Validation

In order to validate the numerical results the shock-detachment distance (δ), and the pressure coefficient maximum (c_{Pmax}) were compared with the results from theory (Table 4).

First, the inviscid 50° cone results were evaluated. The Mach 2.21 case results in a detached shock-wave and therefore a theory considering the existence of a normal shock wave has to be used for the comparison. The modified Newtonian law, which gives c_{Pmax} at a stagnation point behind a normal shock wave seems to be suitable, and the formula (see for example [9]) $c_{Pmax} = \frac{2}{\gamma.M^2}[[\frac{(\gamma+1)^2.M^2}{4.\gamma.M^2-0.8}]^{\frac{\gamma+1}{\gamma-1}}[\frac{(\gamma-1)+(\gamma+1).M^2}{(\gamma+1)}] - 1]$ predicts a value of 1.689, which is in excellent agreement with the CFD prediction. On the other hand, there is no analytical formula available for the shock-detachment distance for cones, and therefore no direct comparison could be done here. The supporting fact is, that the $\theta - \beta - M$ diagram from the conical flows theory results in no intersection for $\theta = 50^o$ and M=2.21 (see [10]), which means that the shock is detached.

From the same sources higher Mach numbers cases yield attached foreshocks, (corresponding to zero values of δ in Table 4) which was correctly predicted by the numerical method (see Figs. 15,20). Therefore, another theory considering no normal portion of shock was employed for the comparison. Rasmussen's formula for c_{Pmax}, derived from the hypersonic small-disturbance theory and plotted in [9] seems to be suitable, even if this reference validated it only up to the value of 30° for the cone half-angle. Nevertheless, extending this to 50° yields a still reasonable agreement with the numerical results, as it can be seen from the second and third row of Table 4.

Mach Num.	Cone Angle	δ_{CFD}	δ_{THE}	c_{Pmax} CFD	c_{Pmax} Theory
2.21	50	0.035	-	1.670	1.689
6.00	50	0	0	1.270	1.249
30.0	50	0	0	1.230	1.232
2.21	90	0.395	0.343	1.682	1.663
6.00	90	0.258	0.257	1.907	1.810
30.0	90	0.247	0.242	1.824	1.832

Table 4: Comparison of the CFD and theoretical results

In the case of the flat nosed cylinder viscous results were compared with analytical ones from [11], where an extensive theoretical analysis is given for high-speed flows over simple blunt bodies. To calculate the shock-detachment distance, the formula $\delta/a = 1.182\sqrt{k}$ from [11] was used, where a is the body radius (0.5 in our case) and k is the ratio of the pressures in front of and behind the shock wave p_1/p_2. This could be easily calculated from the normal shock-wave relations (see for example [9]). As Tab.4 shows, numerical results are almost identical to the theoretical ones apart of the Mach 2.21 case. The slight deviation in this case could be explained by the fact, that the above formula was explored for hypersonic range only, which could cause inaccuracy for a supersonic application. Nevertheless, the values are reasonable.

Finally, the pressure coefficients at the stagnation point were compared with the results from the formula $c_{Pmax} = (2-k)$ [11], where k has the same meaning as above, and as one can see the results are again in very good agreement with the theory.

6 Conclusions and Future Work

To improve the robustness of the PMB2D code and to extend the solvable range of the freestream velocities to very high hypersonic values, two modifications were presented in this paper.

First, a modification to the wall boundary condition was proposed to resolve problems arising from the strong expansion corners of the blunt bodies. As this modification was in use mainly at the beginning of the calculations, its role could be defined as helping the calculations through the initial, crucial parts of the time-marching scheme. However, instabilities in convergence were observed at inviscid, high freestream velocity cases, which reason has not been revealed yet.

The second modification, Harten's entropy fix, was necessary to overcome the resolution problem of the extremely strong bow shock arising over a blunt body at hypersonic speed.

Then, computational results of the high-speed steady flows over a spike, a 50° half angle cone and a flat-nosed cylinder were compared with the theory and a good agreement was obtained. Grid dependence tests showed no effect on the solutions, and therefore it could be stated that the proposed modifications are correct and they improve significantly the robustness of the code. The calculation times, depending on the particular case, were ranging from 13 minutes up to 5 h 30 minutes, which demonstrates the ability of CFD to be a powerful alternative to the experiments when investigating high speed flows over simple shapes.

Furthermore, the above examined simple bodies could be assembled to spiked cone/cylinder, and an attempt to simulate unsteady supersonic/hypersonic flows over spiked bodies could be done.

References

[1] Eggers, A.J., Allen, M.J., "A Study of the Motion and Aerodynamic Heating of Ballistic Missiles Entering the Earth's Atmosphere at High Supersonic Speeds", *NACA TR 1281* 1958.

[2] Minges, M.L., "Ablation Phenomenology (a review)", *High Temperatures-High Pressures, Vol 1,* 1969.

[3] Abbett, M.J., Cooper, L., Dahm, T.J., Jackson, M.D., "Flow Characteristics about Concave Conic Forebodies at High Mach Numbers", *AIAA P 75-153,* 1975.

[4] Kenworthy, M.A., "A Study of Unstable Axisymmetric Separation in High Speed Flows", *PhD Thesis, Virginia Polytechnic Institute and State University,* 1978.

[5] Badcock, K.J., Richards, B.E., "Implicit Time Stepping Methods for the Navier-Stokes Equations", *AIAA Journal, vol 34, no 3, pp. 555-559,* 1996.

[6] Dubuc, L., Cantariti, F., Woodgate, M., Gribben, B., Badcock, K.J., and Richards, B.E., "Solution of the Unsteady Euler Equations Using an Implicit Dual Time Method", *AIAA Journal, vol 36, No 8, pp. 1417-1427,* 1998.

[7] Gribben, B., "Shock Reflection Hysteresis in an Underexpanded Jet", *PhD Thesis, University of Glasgow* 1998.

[8] Gnoffo, P.A., "Point-Implicit Relaxation Strategies for Viscous, Hypersonic Flows", *Computational Methods in Hypersonic Aerodynamics, edited by Murthy, T.K.S., Kluwer Acadamic Publishers, pp. 115-151,* 1993.

[9] Anderson, J.D., Jr., "Hypersonic and High Temperature Gas Dynamics", *McGraw-Hill Book Company, pp. 114-115,* 1989.

[10] Ames Research Staff, "Equations, Tables, and Charts for Compressible Flow", *NACA-TR-1135,* January 1953.

[11] Truitt, R.W., "Hypersonic Aerodynamics", *The Ronald Press Company, New York, pp. 231-296,*1959.